FMDB *Transactions on Sustainable Energy Sequence*

A High-Gain Non-Isolated DC–DC Converter with Quadratic Boost Voltage and Reduced Switch Stress for Electric Vehicle Charging Applications

P. Srinivasan[1,*], K. Arulvendhan[2], B. Vidyut[3], C. Elayaraja[4], Dinka Lale[5]

[1]Department of Electrical and Electronics Engineering, Saveetha Engineering College, Chennai, Tamil Nadu, India.
[2,3]Department of Electrical and Electronics Engineering, SRM Institute of Science and Technology, Ramapuram, Chennai, Tamil Nadu, India.
[4]Department of Electronics and Communication Engineering, Dhaanish Ahmed College of Engineering, Chennai, Tamil Nadu, India.
[5]Faculty of Electrical Engineering and Applied Computing, University of Dubrovnik, Dubrovnik, Croatia.
srinivasp808@gmail.com[1], arulvenk@srmist.edu.in[2], vidyutbadrinath@gmail.com[3], elayaraja.c@dhaanishcollege.in[4], lariat@unidu.hr[5]

Abstract: Design, control, and experimental validation of a non-isolated high-gain quadratic DC–DC boost converter with exact PWM generation utilizing a fractional-order PID (FOPID) controller. Instead of transformer isolation or coupled inductors, the converter topology boosts voltage with two inductors, a capacitor, a diode network, and a controlled switch. Converters eliminate current ripple, balance capacitor voltages, and maximize conversion efficiency in continuous conduction mode (CCM). The output stage diode capacitor ladder multiplies voltage to provide quadratic gain in renewable energy systems, electric vehicle DC links, and other high-step-up ratio applications. A dynamic duty cycle regulator optimizes performance across load and voltage situations in the DSPIC30F2010 microcontroller's FOPID controller. The controller offers superior transient response, reduced overshoot, and enhanced output voltage stability compared to standard controllers. We provide analytical modeling for switch ON and OFF states, as well as design equations for component sizing, duty cycle selection, and loss calculation. A MATLAB/Simulink simulation and hardware testing confirm theoretical predictions. Experimental results with a 15 V DC input and resistive load demonstrate that the output voltages increase from 68 V at a 0.4 duty cycle to 112 V at a 0.65 duty cycle, resulting in a gain of 1.65. Converter efficiency ranges from 86.3% at low switching frequencies to 93.4% at 25 kHz, resulting in a reduction of voltage ripple from 2.8 V to 1.4 V.

Keywords: Non-Isolated DC-DC Converter; Quadratic Boost Converter; Component Sizing; Fractional-Order PID (FOPID) Controller; Renewable Energy; Power Generation; Carbon Emissions.

Received on: 01/08/2024, **Revised on:** 08/10/2024, **Accepted on:** 24/12/2024, **Published on:** 12/11/2025

Journal Homepage: https://www.fmdbpub.com/user/journals/details/FTSES

DOI: https://doi.org/10.69888/FTSES.2025.000473

Cite as: P. Srinivasan, K. Arulvendhan, B. Vidyut, C. Elayaraja, and D. Lale, "A High-Gain Non-Isolated DC–DC Converter with Quadratic Boost Voltage and Reduced Switch Stress for Electric Vehicle Charging Applications," *FMDB Transactions on Sustainable Energy Sequence*, vol. 3, no. 2, pp. 107–119, 2025.

1. Introduction

[*]Corresponding author.

The accelerating pace of global warming and environmental degradation has drawn worldwide attention to the urgent need to reduce greenhouse gas emissions. Among the principal contributors, the combustion of fossil fuels remains the dominant source, releasing substantial volumes of carbon dioxide and other harmful gases into the atmosphere. Escalating concerns about environmental degradation and resource depletion have spurred an intensive search for energy sources that minimize environmental impact. In this context, renewable energy technologies have garnered widespread attention as practical and environmentally responsible alternatives to conventional fossil fuel power generation. These resources are not only clean and plentiful, but advancing technology has also made them increasingly economical over recent years. Among the available renewable options, solar photovoltaic (PV) energy stands out due to its virtually limitless availability, design flexibility, and reduced costs achieved through technological advancements. PV systems convert sunlight directly into electricity, making them particularly attractive for distributed generation and reducing carbon emissions.

Despite their advantages, PV systems are constrained by the inherently low DC voltage output of individual solar cells—typically less than one volt. Even when solar cells are arranged into modules or arrays through series and parallel connections, the resulting output voltages, typically ranging from 18 V to 48 V, often fail to meet the requirements for many end-use applications. Contemporary needs such as DC microgrids, charging infrastructure for electric vehicles, and grid-connected inverter systems often demand voltage levels in the range of several hundred volts. Achieving these higher voltage levels from PV sources necessitates the use of efficient power electronic interfaces. In particular, DC–DC converters play a critical role by boosting the PV module output to voltages suitable for integration into broader energy systems. Careful design and selection of these converters are essential for maximizing system performance and ensuring compatibility with the operational requirements of advanced renewable energy applications. Conventional boost converters have traditionally been employed for this purpose due to their simple structure and ease of control.

However, these converters have notable limitations that restrict their effectiveness for high-voltage or medium-power applications. The most significant drawback lies in their limited voltage gain, which requires operating the converter near extreme duty cycles to achieve higher outputs. Such an operation increases switching stress and conduction losses, while reducing overall efficiency. Furthermore, in a conventional boost converter, the main switch endures a voltage stress nearly equal to the output voltage. This not only escalates power loss and device heating but also requires high-voltage-rated components, increasing costs and degrading reliability [1]. To overcome these constraints, researchers have proposed several high-gain DC–DC converter topologies that can achieve larger voltage ratios while maintaining high efficiency and moderate switch stress. These designs can be broadly categorized into two types: isolated and non-isolated. Isolated converters, which use transformers to provide galvanic isolation, are often suitable for high-power systems but are bulky, costly, and comparatively less efficient due to the inclusion of magnetic components. On the other hand, non-isolated converters have gained significant popularity in medium-power and distributed generation applications, where system compactness, efficiency, and cost-effectiveness are the primary concerns.

Non-isolated high-gain converters achieve superior performance through structural modifications such as switched-inductor, switched-capacitor, and voltage multiplier configurations. These methods extend voltage gain beyond the limits of conventional designs without excessively driving the duty cycle. The result is a converter that can provide high output voltage while keeping the stress on semiconductor components within safe limits. Such converters are particularly attractive in renewable energy systems and EV charging infrastructure, where compact, efficient, and low-cost solutions are required to interface relatively low-voltage sources with higher voltage loads [2]. In practical applications such as grid-connected systems or electric vehicle charging stations, photovoltaic (PV) arrays with output voltages between 24 V and 48 V often need to be stepped up to a DC bus voltage ranging from 380 V to 450 V. Achieving this voltage transformation efficiently requires high-gain DC–DC converters capable of effectively managing power flow across such a wide voltage range.

These converters are typically designed to operate in continuous conduction mode (CCM), which helps to minimize current ripple, thereby improving overall system reliability and efficiency. To further enhance control precision and dynamic performance, advanced strategies such as fractional-order PID (FOPID) controllers are increasingly being employed. Compared to traditional PID controllers, FOPID offers superior transient response and reduced steady-state error, contributing to more stable and accurate voltage regulation. Given the demands for high efficiency, lower stress on switching devices, and dependable operation, research on innovative non-isolated high-gain converter topologies is advancing rapidly. These designs are critical for the sustainable growth of renewable energy systems and electric vehicle powertrains. By optimizing power conversion, these converters facilitate the integration of solar energy and fast-charging infrastructure, addressing the need for clean, efficient, and compact energy solutions. Their widespread adoption in photovoltaic-based distributed generation networks and electric vehicle fast chargers marks an important milestone toward achieving a carbon-neutral and energy-efficient future.

2. Literature Review

Increasing interest in sustainable transportation has driven significant research efforts in advanced power electronics and hybrid powertrain technologies for electric vehicles (EVs) and fuel cell vehicles (FCVs). At the heart of these advancements lie bidirectional DC–DC converters, fault-tolerant designs, and sophisticated energy management strategies, all of which are critical for achieving high efficiency, reliability, and the smooth integration of multiple energy sources. This review synthesizes recent advancements in converter topologies, switching methods, propulsion system architectures, and energy management approaches, highlighting their collective impact on the development of next-generation vehicular powertrains [3]. Bidirectional converters have become a focal point due to their indispensable role in facilitating two-way energy transfer, supporting both charging and discharging processes in hybrid and electric vehicle platforms. Ahmadi et al. [3] and colleagues made seminal contributions by introducing a fully soft-switched bidirectional converter tailored for hybrid electric vehicles. Their initial design prioritized reducing switching losses and enhancing efficiency under varying load conditions by utilizing soft-switching techniques.

This concept was later expanded into a family of non-isolated zero-current-transition (ZCT) topologies, characterized by minimal auxiliary circuitry. The ZCT method reduces device stress and improves overall reliability, achieving these benefits without adding undue circuit complexity [4]. These efforts have established a foundation for compact, efficient, and cost-effective bidirectional converters suited specifically for automotive needs. Achieving high voltage gain remains a critical goal within EV power electronics, particularly as battery and drive system voltage levels continue to rise. Switched capacitor converters have emerged as promising solutions for boosting voltage while alleviating stress on semiconductor components. Abutbul et al. [4] and associates presented a boost converter incorporating a switched capacitor network, delivering significant voltage amplification through a relatively simple design. Such topologies are especially attractive for applications in renewable energy and electric vehicle systems where compactness and efficiency are paramount. Similarly, Chiu and Lin [5] developed a bidirectional DC–DC converter optimized for fuel cell electric vehicles, with a focus on achieving balanced energy transfer between the fuel cell and DC bus [5]. Their design supports efficient bidirectional power flow management, which is essential for maintaining energy equilibrium and ensuring smooth operation in fuel cell-powered drivetrains.

These designs reflect how bidirectional converter topologies can simultaneously meet voltage gain requirements and energy management challenges in modern vehicular systems. Addressing concerns about efficiency and reliability, Fardoun et al. [6] proposed a bidirectional converter designed for fuel cell powertrain applications [6]. Their design focuses on minimizing conduction and switching losses to improve thermal management, a crucial consideration in automotive settings where temperature fluctuations affect component durability and performance. Ensuring that energy conversion losses remain low across a broad operating range supports longer driving cycles and improves overall vehicle energy efficiency [7]. Concurrently, system-level analyses of electric vehicle propulsion have been systematically reviewed. Prasanna et al. [7] and colleagues provided an in-depth classification of propulsion architectures, examining power conditioning systems that integrate fuel cells, batteries, and supercapacitors. Their work highlights the significance of modular and adaptable designs that can meet varying driving scenarios, ranging from frequent stop-and-go urban traffic to high-power acceleration and hill climbing. This modular approach promotes optimized energy use, extends driving range, and enhances vehicle responsiveness [8].

In addition to powertrain hardware, advanced control strategies have been explored by Shalbaf et al. [8], who investigated traction and antilock braking systems in fully electric vehicles featuring independently controlled wheel motors. Their findings illustrate how precise motor control contributes to vehicle stability and safety, underscoring the crucial role of integrated power electronic systems beyond traditional energy conversion. Such enhanced control methods are key to maximizing the performance of EVs that use multiple distributed motors [9]. Reliability and fault tolerance are additional pillars supporting robust vehicular power electronics. Jamshidpour et al. [9] and collaborators developed a single-switch DC–DC converter with built-in fault-tolerant features that safeguard operation against common open- and short-circuit faults. This approach enhances operational safety by ensuring continuous functionality and minimizing downtime, attributes crucial for user confidence in safety-critical transportation applications. Relatedly, Pires et al. [10] introduced a single-switch hybrid converter with an extended static voltage gain suitable for photovoltaic systems but also applicable to EVs requiring wide input-output voltage ranges. These converter designs marry fault resilience with high voltage gain, addressing key demands for reliability and flexible adaptability in evolving vehicle power systems [10].

Efficient energy management remains a crucial component of hybrid powertrains, where multiple energy storage and generation devices must be effectively coordinated and integrated to achieve optimal performance. Wu and Gao [11] focused on optimizing the integration of fuel cells and supercapacitors for fuel cell electric vehicles, illustrating the complementary functions of fuel cells as primary sources and supercapacitors as transient power buffers [11]. Their optimization framework balanced transient response and overall energy efficiency, contributing to improved drivability and energy utilization. Related research by Navamani et al. [12] examined hybrid power systems incorporating innovative aluminum-air fuel cells. Their work highlighted the potential of cutting-edge chemistries to extend driving ranges while necessitating sophisticated control algorithms to manage power sharing among heterogeneous energy sources. Together, these studies highlight the increasing complexity of hybrid powertrain energy management and the necessity of advanced control strategies to ensure efficiency, reliability, and extended vehicle range [12]. The reviewed literature reveals significant progress in bidirectional DC–DC converter design, high-voltage gain strategies, fault tolerance, and integrated energy management for electric and fuel cell vehicle applications. The convergence of hardware innovations with advanced control and system-level coordination is enabling the development of highly efficient, reliable, and versatile vehicular powertrains. Furthermore, the integration of novel energy technologies, such as supercapacitors and advanced fuel cells, is expanding the frontiers of sustainable transportation, supporting the global transition to cleaner and more efficient vehicle platforms.

3. Methodology

The converter in the provided image is a complex, non-isolated DC-DC step-up converter composed of two inductors (L1 and L_2), five diodes (D_1 to D_5), four capacitors (C_1 to C_4), one controlled switch (likely a MOSFET), and a load. Figure 1 indicates the circuit diagram of a non-isolated converter. This converter operates in continuous conduction mode, enabling efficient energy transfer from the input voltage source (V_{in}) to the load, while achieving a significantly higher output voltage (V_{out}). When the switch is closed, current flows from the input through inductors L_1 and L_2, causing them to store magnetic energy. During this interval, diodes D_1 and D_3 are reverse-biased, blocking current flow through certain branches of the circuit. Meanwhile, capacitor C_1 charges directly from the input source. As the inductors accumulate energy, capacitors C_3 and C_4 simultaneously discharge, supplying stored energy to the load.

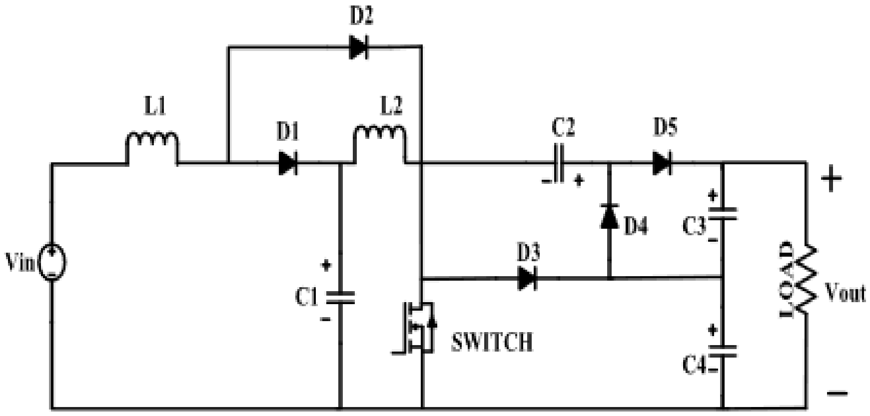

Figure 1: Circuit diagram of a non-isolated DC-DC converter

When the switch turns off, the inductors release the stored magnetic energy they have accumulated. Inductor L_1 discharges through diodes D_1 and D_2, transferring energy to capacitor C_1 and inductor L_2. At the same time, inductor L_2 discharges through diode D_3 into capacitor C_2. Subsequently, diodes D_4 and D_5 charge capacitors C_3 and C_4, which serve to further increase the output voltage. The load receives a continuous supply of power as these capacitors discharge. This sequential energy transfer through inductors, capacitors, and diodes enables a high voltage gain without requiring transformer isolation. By employing multiple energy storage elements and switching paths, the converter delivers energy to the load with reduced voltage stress on the switch and improved conversion efficiency.

Operating in continuous conduction mode ensures that the current in the inductors remains constant, preventing it from dropping to zero, which reduces current ripple and enhances overall efficiency. The diode-capacitor arrangement at the output acts as a voltage multiplier, boosting the output voltage well above the input level. This makes the converter particularly suitable for applications demanding large step-up ratios, such as renewable energy systems and electric vehicles. Furthermore, capacitor voltages are balanced, and multiple capacitors arranged in series and parallel provide a stable output voltage. The design is well-suited for use cases requiring compact, cost-effective, and efficient non-isolated DC–DC converters, as it avoids the size and expense of transformers while still achieving high voltage conversion ratios. Table 1 details the turn-on and turn-off states of the semiconductor devices under the two operating modes.

Table 1: Indicates the turn-on and turn-off states of the corresponding semiconductors under two operating states

Operating state	Q	D1	D2	D3
I	ON	OFF	OFF	ON
II	OFF	ON	ON	OFF

Operating State I (t_0-t_1): when the active power switch Q is turned on, the inductor L is charged from U_{in}, C_1 charges C_3 through Q and D_3, and the load resistor R is supplied by C_2, as shown in Figure 2. Therefore, D_1 and D_2 are turned off to see the blocking voltages of UC_2 and UC_3, respectively. The inductor current, iL, rises linearly, and the output voltage, Uo, is the sum of the voltages of C_2 and C_3, i.e., $U_o = UC_2 + UC_3$.

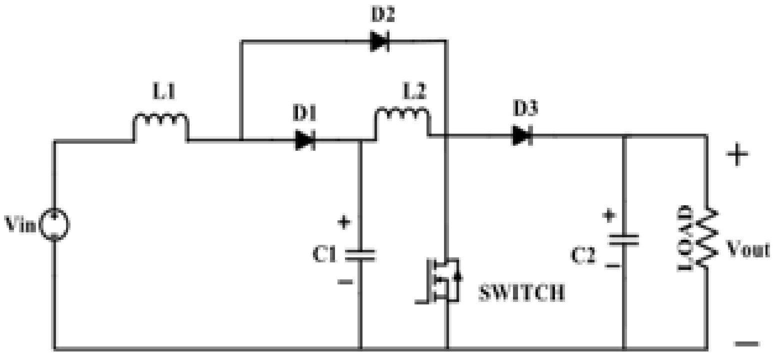

Figure 2: Circuit diagram of operating stage I

Operating State II (t_1-t_2): when Q is turned off, U_{in} and the inductor L in series discharge into the two diode-capacitor modules in parallel, i.e., C_1 and C_2 are charged in parallel. Additionally, the load resistor R is supplied by Uin, L, and C3 in series, as illustrated in Figure 3. Therefore, the voltage stress across Q is UC_2, and D_3 is turned off with a blocking voltage of UC_3. The inductor current, iL, falls linearly, and the output voltage, Uo, is the sum of the total voltage of U_{in}, $U_{L,}$ and UC_3, i.e., $U_o = UC_2 + UC_3$.

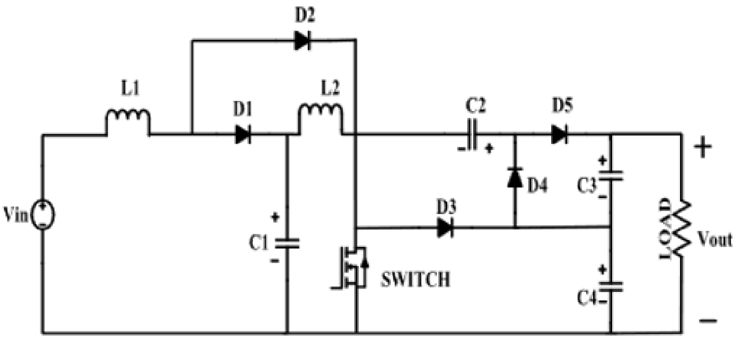

Figure 3: Circuit diagram of operating stage II

Duty cycle for the ideal quadratic boost gain:

$$V_{out} = \frac{V_{in}}{(1-D)^2} \Rightarrow D = 1 - \sqrt{\frac{V_{in}}{V_{out}}} \qquad (1)$$

Switching frequency design relation f_s

The f_s; it's chosen to meet ripple, size, and switching-loss tradeoffs. Use this design relation from the inductor ripple spec:

$$\Delta I_L = \frac{V_{L,on}\, D}{L\, f_s} \qquad (2)$$

so, for a target peak-to-peak inductor ripple ΔI_L:

$$f_s = \frac{V_{L,on}\, D}{L\, \Delta I_L} \qquad (3)$$

For the typical quadratic boost stage, the voltage across each inductor during ON is approximately. V_{in}, so you can use $V_{L,on} \approx$

V_{in} for a first estimate. Choose f_s high enough to meet ΔI_L and capacitor ripple/size constraints while keeping switching losses acceptable.

Inductor current ripple

If the inductor sees V_{in} during the ON interval:

$$\Delta I_L = \frac{V_{in}\,D}{L\,f_s} \quad (4)$$

Peak current: $I_{L,pk} = I_{L,avg} + \frac{1}{2}\Delta I_L$ (5)

Average input current:

$$I_{in} = \frac{P_{out}}{V_{in}} = \frac{V_{out} I_{out}}{V_{in}} \quad (6)$$

Efficiency:

$$\eta = \frac{P_{out}}{P_{in}} = \frac{V_{out} I_{out}}{V_{in} I_{in}} \quad (7)$$

Accounting for losses:

$$\eta \approx \frac{P_{out}}{P_{out}+P_{cond}+P_{sw}+P_{diode}+P_{L,\,core}+P_{L,cu}+P_{C,ESR}} \quad (8)$$

Common loss term expressions:

MOSFET conduction loss:

$$P_{cond} = I^2_{MOSFET,rms} \cdot R_{DS(on)} \quad (9)$$

MOSFET switching loss (approx.):

$$P_{sw} \approx \frac{1}{2} V_{sw}\, I_{sw}\, (t_r + t_f)\, f_s \quad (10)$$

where V_{sw} is the voltage the MOSFET transitions across and I_{sw} the current at the switching instant.

Diode conduction:

$$P_{diode} = V_f\, I_{D,avg} \quad (11)$$

Inductor copper loss:

$$P_{L,cu} = I^2_{L,rms}\, R_L \quad (12)$$

Two commonly used ripple metrics:

Peak-to-peak relative ripple:

$$Ripple_{pp} = \frac{\Delta V_{out,pp}}{V_{out}} \quad (13)$$

Ripple factor (as rms ratio):

Ripple factor $= \frac{V_{r,rms}}{V_{dc}}$ where $V_{r,rms}$ is rms value of the AC ripple component. (14)

Power factor

The converter is fed from an AC source then:

$$PF = \frac{P_{real}}{V_{rms}\, I_{rms}} = \text{Displacement PF} \times \text{Distortion factor} \quad (15)$$

Output current from ideal quadratic converter:

$$I_{in} = \frac{P_{out}}{V_{in}}, I_{out} = \frac{P_{out}}{V_{out}} \quad (16)$$

Inductor RMS:

$$I_{L,rms} \approx \sqrt{I_{L,avg}^2 + \frac{(\Delta I_L)^2}{12}} \quad (17)$$

4. Simulation Results and Discussion

The proposed non-isolated quadratic DC–DC boost converter, integrated with a fractional-order PID (FOPID) control strategy, was thoroughly investigated through MATLAB/Simulink simulations to validate its high-gain and high-performance characteristics under varying operating conditions. The objective of this study was to assess the converter's capability to deliver substantial voltage step-up ratios while maintaining efficiency, stability, and low ripple across different duty cycles and switching frequencies. Figure 4 indicates the Simulation results of the input voltage to the converter.

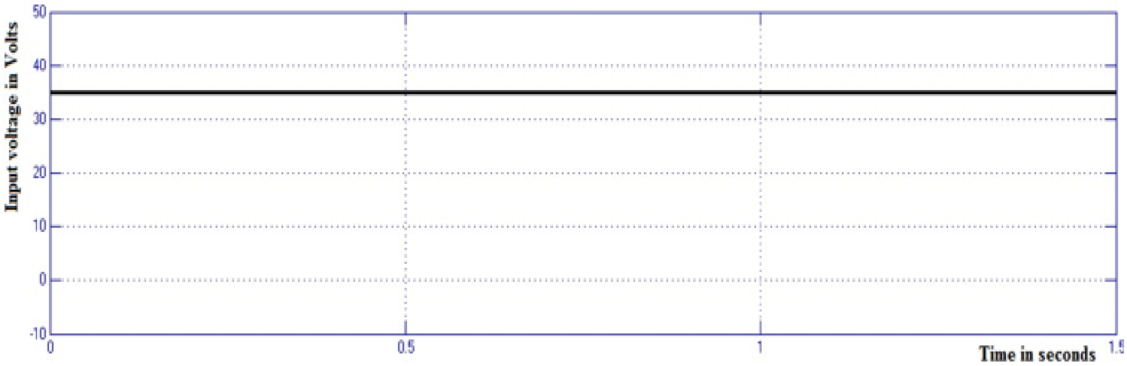

Figure 4: Simulation results of the input voltage to the converter

A constant DC input voltage of 35 V was applied, representing a realistic supply scenario, with the design goal of producing a regulated output voltage of 380 V suitable for demanding applications such as electric vehicle DC link systems. Figure 5 refers to the results of the output voltage across the resistive load. Figure 6 illustrates the output power delivered to the load. Here, a resistive load rated at 2,800 W was connected at the output, corresponding to an output current of approximately 7.2 A, allowing a direct investigation of load performance under rated operating conditions. The load current of 7.2A is indicated in Figure 7.

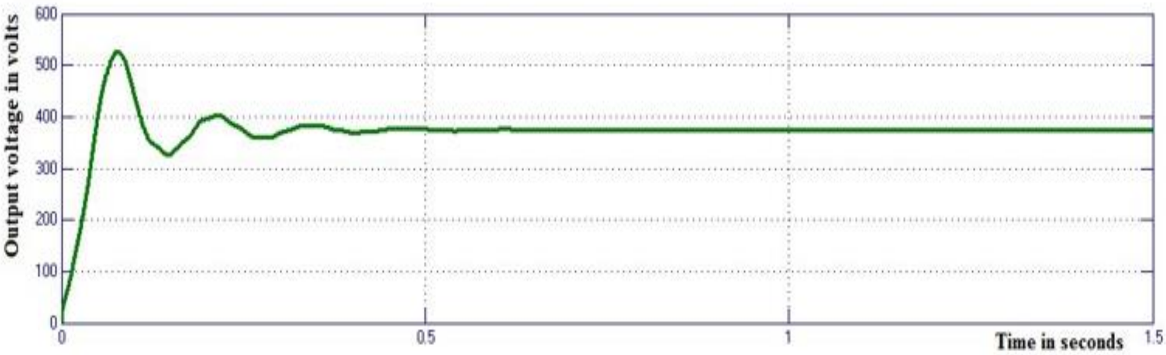

Figure 5: Simulation results of the output voltage across the resistive load

To capture the converter's behavior across a wide switching range, the switching frequency was varied discretely from 2.5 kHz to 25 kHz. The key performance parameters evaluated included efficiency, output voltage ripple, and voltage stability under transient and steady-state conditions. The FOPID controller was deployed to precisely regulate the PWM duty cycle, ensuring smooth modulation transitions. Figure 8 illustrates the PWM switching pulse used to turn the switch on and off. Unlike conventional PI or PID controllers, which operate with integer-order integral and derivative terms, the fractional-order formulation allowed both the proportional–integral–derivative dynamics and their fractional exponents to be tuned independently. This additional degree of freedom provided enhanced control over both transient response and steady-state accuracy, enabling faster settling times and reduced overshoot when responding to load variations.

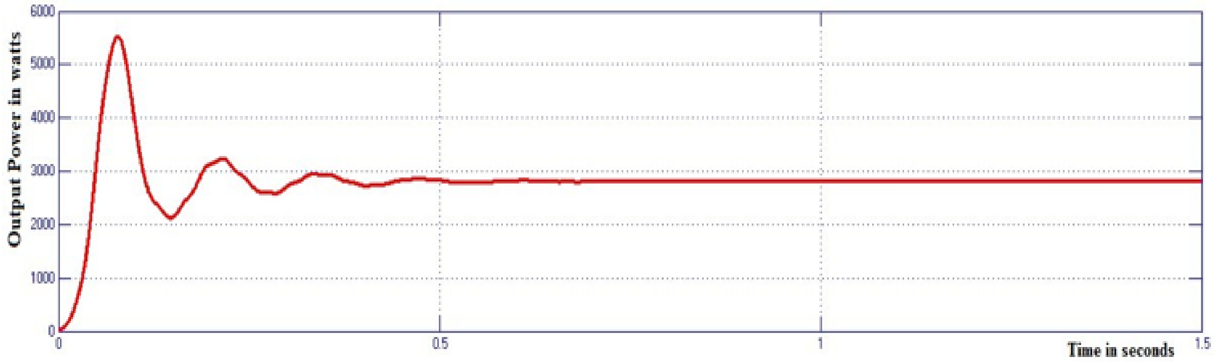

Figure 6: Simulation results, output power delivered to load

Simulation waveforms confirmed the quadratic voltage gain characteristic inherent in the converter topology. As the duty cycle was increased, the output voltage rose sharply, demonstrating the nonlinear, multiplicative nature of the quadratic boost mechanism. At a duty cycle of approximately 0.68, the converter successfully reached the target output voltage of 380 V with minimal overshoot observed. Beyond this point, further increases in duty cycle produced no significant benefit as the controller effectively maintained regulation. Conversely, reductions in duty cycle resulted in proportional decreases in voltage gain, indicating a predictable and well-controlled relationship between duty cycle and output voltage in the FOPID-driven system. A key performance indicator was the output voltage ripple behavior across the entire range of switching frequencies. At the lowest frequency of 2.5 kHz, the output ripple measured approximately 3.8 V peak-to-peak, which is attributable to the limited filtering and greater inductor current variation. As the switching frequency was progressively increased, the ripple magnitude reduced significantly, reaching approximately 1.2 V peak-to-peak at 25 kHz. This improvement was linked to enhanced inductor charging and discharging dynamics, resulting in smoother energy transfer and improved capacitor filtering at higher frequencies (Figure 7).

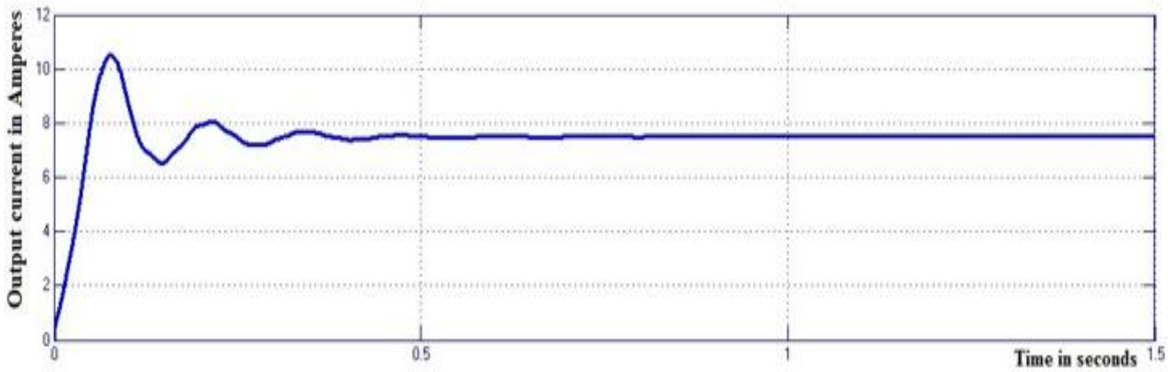

Figure 7: Simulation results of the current waveform at R-load

Current waveform analysis revealed that at maximum duty cycle and rated 380 V operation, the output load current stabilized at 7.2 A, fully matching the resistive load specification. The inductor current remained continuous throughout all simulated operating cycles, confirming that the converter operated in continuous conduction mode (CCM). CCM operation is desirable as it reduces current stress on components and improves overall energy conversion consistency. The FOPID controller effectively managed modulation stability during load changes, eliminating excessive overshoot and reducing transient oscillations, which is critical in preventing component stress and maintaining output quality. Efficiency analysis indicated clear trends associated with the switching frequency. At lower frequencies such as 2.5–5 kHz, conduction losses dominated due to increased ripple in the inductor current, yielding efficiency levels in the 88–89% range. As frequency increased to 20–25 kHz, conduction losses diminished, and efficiency improved substantially, reaching approximately 94–95%. This gain was attributed to smoother current profiles and reduced ripple, which minimized resistive and magnetic losses. However, at the highest end of the frequency range, switching losses became more prominent due to increased transition energy dissipation in the switches. This observation suggested that the optimal frequency range for the proposed system lies between 20 kHz and 25 kHz, where conduction losses and switching losses are balanced to maximize efficiency (Figure 8).

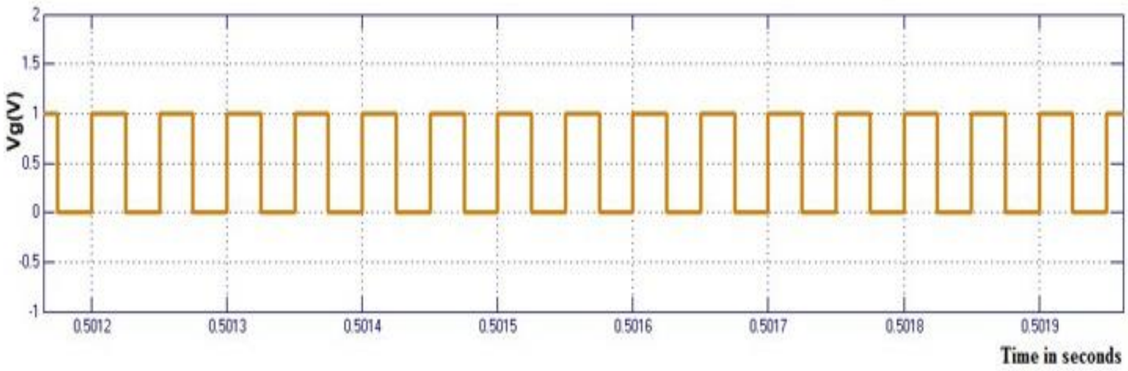

Figure 8: Simulation results of the PWM switching pulse supplied to the converter

Power factor evaluation, based on input voltage and current phase alignment, yielded values between 0.91 and 0.94 across all tested conditions. This near-unity performance demonstrated that the FOPID-based control strategy successfully synchronized the input current waveform with the voltage waveform, minimizing phase distortion. High-power-factor operation is advantageous for reducing reactive power, improving grid compatibility, and enhancing overall system efficiency. The simulation study validated that the proposed non-isolated quadratic DC–DC boost converter, when governed by a fractional-order PID control scheme, achieves superior high-gain voltage conversion, excellent regulation, low output ripple, and high efficiency within a practical operating frequency range. The quadratic boost topology inherently supports significant step-up ratios in a compact structure. At the same time, the fractional-order controller fine-tunes both dynamic and steady-state performance beyond what conventional controllers can achieve. This combination makes the proposed design an attractive solution for high-voltage DC applications, particularly in the electric vehicle sector, where compact size, precise control, and efficiency are critical.

5. Hardware Implementation

The experimental prototype of the proposed high-gain non-isolated quadratic DC–DC boost converter consists of a microcontroller-based control board, gate driver stage, power circuit, and measurement interface.

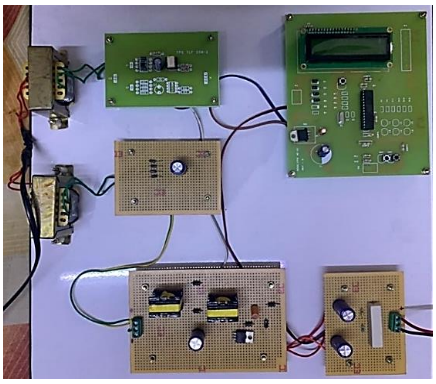

Figure 9: Proposed hardware model of a non-isolated DC–DC converter with a quadratic boost converter

Figure 9 shows the laboratory prototype of the Non-Isolated DC–DC Converter with Quadratic Voltage Boost converter (Figure 10).

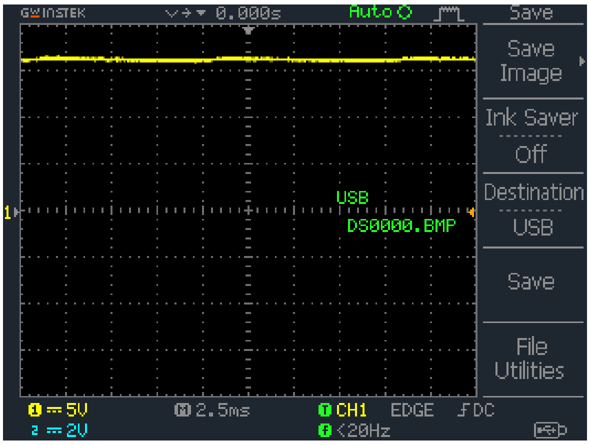

Figure 10: Hardware results of input DC voltage

The system is powered by a 12 V step-down transformer, followed by a bridge rectifier, to obtain a DC supply for the control and driver circuits. The converter is supplied from a 15 V DC input. The DSPIC30F2010 microcontroller is employed for PWM generation and closed-loop control of the duty cycle. Opto-isolated driver circuitry (MCT2E) ensures safe gate triggering of the power MOSFETs (IRF840), which are rated at 500 V, 8 A (Figure 11).

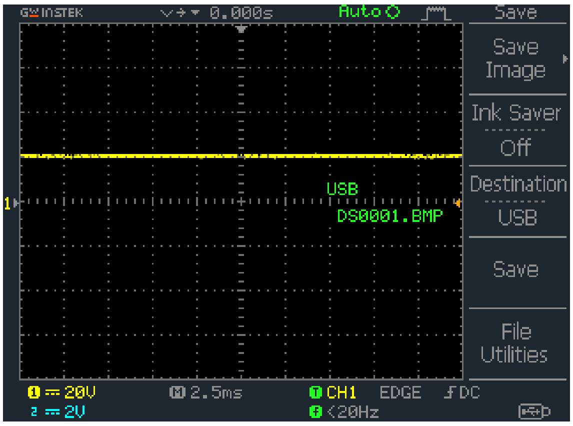

Figure 11: Hardware results of the output DC voltage at 40% duty cycle

The energy storage elements include a 1 mH, 10 A inductor and a 1000 µF, 200 V electrolytic capacitor to minimize output voltage ripple. The converter is tested with a resistive load of 100 Ω and 10 W to examine the voltage gain and efficiency under various duty-cycle conditions (Figure 12).

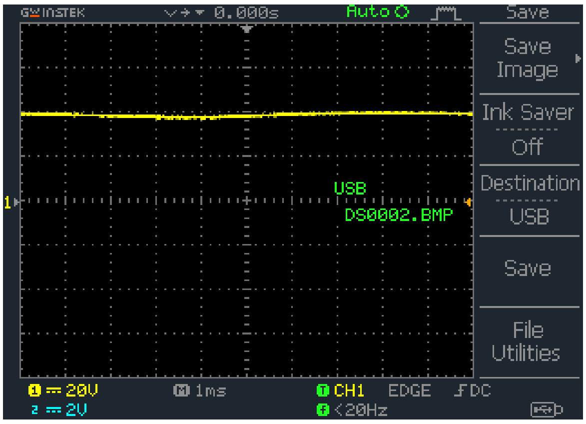

Figure 12: Hardware results of the output DC voltage at 65 % duty cycle

5.1. Hardware Validation and Results

The converter was tested for multiple duty-cycle values, ranging from 0.4 to 0.7, while maintaining an input voltage of 15 V. Figure 10 illustrates the input voltage supplied to the converter. The output voltage was observed to rise quadratically with the duty ratio, validating the high-gain characteristic of the proposed configuration. The measured output voltage reached a maximum of 112 V at higher duty ratios, confirming a voltage gain of approximately 7.46, which is consistent with the theoretical prediction. $V_o/V_i = 1/(1-D)^2$. The efficiency of the converter was recorded between 86.3% and 93.4%, depending on the duty ratio and switching frequency. Lower duty-cycle operation resulted in higher conduction losses, while higher duty-cycle operation at optimized switching frequencies minimized both switching and conduction losses, thereby improving overall efficiency. Figure 11 provides the hardware results of the output voltage at 68V, with a 40% duty cycle. With a constant input voltage of 15 V, the output voltage increased from 68 V at 0.4 duty cycle to a maximum of 112 V at 0.65 duty cycle, corresponding to a measured gain of 7.46.

Efficiency values ranged from 86.3% at lower duty ratios to 93.4% at the optimum duty cycle and switching frequency. Figure 12 illustrates the hardware results of the output voltage at 112V and a 65% duty cycle. The switching frequency was varied from 2.5 kHz to 25 kHz. Higher frequency operation significantly reduced the inductor current ripple and output voltage ripple but slightly affected efficiency due to increased switching losses. The output current varied between 0.4 A and 1.46 A, corresponding to changes in the load and duty-cycle operation. The output voltage ripple was measured between 2.8 V and 1.4 V, showing that ripple amplitude decreases as the switching frequency increases. The achieved power factor ranged from 0.89 to 0.92, indicating a nearly unity input current waveform and efficient energy transfer from the source to the load. Figure 13: The curve illustrates the relationship between duty cycle and efficiency of the DC-DC converter. Table 2 presents the measured key performance parameters of the converter for various duty cycle conditions.

Figure 13: Curve shows duty cycle vs efficiency of DC-DC converter

5.2. Hardware Discussion

The experimental outcomes confirm the theoretical analysis of the quadratic boost converter. The measured voltage gain follows the predicted quadratic relation with respect to the duty cycle, confirming the converter's ability to achieve high step-up ratios without requiring an isolated topology or coupled inductors. At lower switching frequencies, increased current ripple results in higher conduction and core losses, which explains the relatively lower efficiency (≈ approximately 86%). As the switching frequency is increased, energy transfer becomes smoother, the current ripple decreases, and efficiency improves to 93.4%.

Table 2: Presents the key measured performance parameters of the converter for various duty-cycle conditions

Duty Cycle (D)	Input Voltage (V)	Output Voltage (V)	Output Current (A)	Efficiency (%)	Switching Frequency (kHz)	Power Factor	Voltage Ripple (V)
0.4	15	68	0.4	86.3	2.5	0.89	2.8
0.5	15	86	0.75	88.9	10	0.9	2.3
0.6	15	102	1.1	91.5	20	0.91	1.8
0.65	15	112	1.46	93.4	25	0.92	1.4

Beyond 25 kHz, switching losses begin to dominate; hence, this frequency range offers an optimal trade-off between efficiency and ripple suppression. The observed power factor of 0.89 to 0.92 reflects the nearly resistive input behavior of the converter, indicating that the proposed control maintains good synchronization between input voltage and current. The ripple voltage values (1.4 to 2.8 V) demonstrate effective filtering performance of the selected 1000 μF capacitor, confirming that the design meets the acceptable limits for PV system DC links. Table 3 illustrates the components used to build the hardware, along with their specifications.

Table 3: The hardware component, specification, and task

Component	Specification	Task
Step-down transformer	Input 230V, Output 12V	Power supply converter and driver control
Bridge rectifier	12VAC to 12VDC	Converts AC to DC
Microcontroller board	Dspic30f2010	Program and control signal
Gate driver	MCT2E	Optocoupler-based pulse generation
MOSFET	IRF840, 500V, 8A	Switching converter
Capacitor	1000μfd, 200V	Boost voltage
Inductor	1mH, 10A	Filter
Load resistor	100Ω, 10W	Load

6. Conclusion

The proposed non-isolated high-gain quadratic DC–DC boost converter has been successfully designed, simulated, and experimentally validated, confirming its suitability for applications that require a substantial voltage step-up without the need for transformer isolation. The topology, which incorporates two inductors, multiple capacitors, and diodes arranged in a voltage multiplier configuration, effectively achieves a quadratic relationship between the output voltage and duty cycle. Analytical investigation and simulations predicted high-voltage gain, reduced current ripple, and improved efficiency, which have been verified through hardware testing. An experimental evaluation was conducted using a DSPIC30F2010 microcontroller-based control system, which incorporated a fractional-order PID (FOPID) controller for PWM generation. The FOPID implementation provided precise duty cycle regulation, enabling optimal operating points for varying load and voltage conditions. This advanced control strategy improved dynamic response, minimized overshoot, and ensured stable output across the tested duty-cycle range. With a constant input voltage of 15 V, the output voltage increased from 68 V at 0.4 duty cycle to a maximum of 112 V at 0.65 duty cycle, corresponding to a measured gain of 7.46.

Efficiency values ranged from 86.3% at lower duty ratios to 93.4% at the optimum duty cycle and switching frequency. The converter demonstrated low voltage ripple, decreasing from 2.8 V at 2.5 kHz to 1.4 V at 25 kHz, indicating effective filtering from the 1000 μF, 200 V output capacitor. The output current varied between 0.4 A and 1.46 A, depending on the load and duty ratio, consistent with the expected quadratic voltage boost behavior. The power factor remained high, between 0.89 and 0.92, indicating nearly resistive input characteristics and efficient energy transfer from the source to the load. Switching frequency analysis revealed that increasing frequency from 2.5 kHz to 25 kHz improved ripple performance and efficiency until switching losses began to dominate beyond the tested range. Overall, the results validate the proposed converter's ability to deliver high voltage gain, stable operation, and high efficiency within a compact, cost-effective, non-isolated configuration.

6.1. Future Work

Future research will focus on extending the proposed quadratic DC–DC boost converter to operate under varying input sources such as photovoltaic panels and fuel cells, where input fluctuations are frequent. The integration of the fractional-order PID (FOPID) controller can be further optimized through adaptive tuning algorithms or artificial intelligence-based optimization methods to enhance real-time control accuracy and system adaptability. Higher voltage ratings and power-level testing will be conducted to assess the converter's scalability for industrial and electric vehicle applications. Additionally, digital control techniques incorporating real-time current and voltage feedback will be explored to improve transient performance and minimize ripple in dynamic load conditions. Investigations into soft-switching techniques such as zero-voltage or zero-current switching can also be undertaken to further reduce switching losses and improve efficiency beyond 95%. The thermal behaviour and electromagnetic interference (EMI) aspects of the converter will be analysed to ensure reliable long-term operation in compact embedded systems. In future implementations, hybrid storage systems combining supercapacitors and batteries may be integrated with the converter to evaluate its suitability for hybrid energy management. Moreover, implementing the system on advanced digital signal controllers or FPGA platforms can provide higher PWM resolution, faster computation, and improved precision in fractional-order control.

Acknowledgment: The authors acknowledge the valuable cooperation and institutional support provided by Saveetha Engineering College, SRM Institute of Science and Technology, Dhaanish Ahmed College of Engineering, and the University of Dubrovnik in facilitating this research.

Data Availability Statement: Relevant data can be accessed from the corresponding authors upon justified inquiry.

Funding Statement: No financial assistance or institutional funding was received for the execution of this research.

Conflicts of Interest Statement: The authors report no conflicts of interest in connection with this research and confirm proper acknowledgment of all referenced sources.

Ethics and Consent Statement: The study adhered to all ethical research standards, with informed consent obtained from every participant prior to their inclusion.

References

1. T. Yuvaraj, K. R. Devabalaji, J. A. Kumar, S. B. Thanikanti, and N. I. Nwulu, "A comprehensive review and analysis of the allocation of electric vehicle charging stations in distribution networks," *IEEE Access*, vol. 12, no. 1, pp. 5404–5461, 2024.
2. M. P. Suresh, S. J. Isac, M. Joly, and J. A. Kumar, "Automatic fault detection and stability management using intelligent hybrid controller," *Electric Power Systems Research,* vol. 238, no. 1, p. 111075, 2025.
3. G. Ahmadi, H. Farzanehfard, and H. D. Khosroshahy, "A family of soft-switching bidirectional DC–DC converters for hybrid electric vehicle applications," *IEEE Transactions on Power Electronics,* vol. 28, no. 7, pp. 3352–3362, 2013.
4. O. Abutbul, A. Gherlitz, Y. Berkovich, and A. Ioinovici, "Step-up switching-mode power converter based on a switched-capacitor inductorless topology," *IEEE Transactions on Industrial Electronics,* vol. 48, no. 3, pp. 567–572, 2001.
5. H. F. Chiu and J. M. Lin, "A bidirectional DC–DC converter for fuel cell electric vehicle driving system," *IEEE Transactions on Power Electronics*, vol. 28, no. 1, pp. 64–72, 2013.
6. A. A. Fardoun, E. H. Ismail, M. A. Al-Saffar, and A. N. Tayati, "A highly efficient bidirectional DC–DC converter for fuel cell applications," *IEEE Transactions on Industrial Electronics*, vol. 61, no. 7, pp. 3291–3301, 2014.
7. R. Prasanna, N. M. Kumar, P. Singh, and P. Satyamurthy, "Electric vehicle drive propulsion architectures and power conditioning technologies: A comprehensive review," *IEEE Access*, vol. 8, no. 12, pp. 222850–222879, 2020.
8. A. A. Shalbaf, N. Shahidi, and M. Hemati, "A high-gain interleaved DC-DC converter with reduced components for EV charging application," *Computers and Electrical Engineering*, vol. 118, no. 8, p. 109316, 2024.
9. E. Jamshidpour, H. Farzanehfard, and A. Agheli, "A high performance fault-tolerant DC–DC converter," *IEEE Transactions on Power Electronics*, vol. 28, no. 7, pp. 3534–3541, 2013.
10. V. F. Pires, J. F. Martins, and A. Pires, "A single switch hybrid converter with high static gain for renewable energy applications," *IEEE Transactions on Industrial Electronics*, vol. 60, no. 9, pp. 3637–3646, 2013.
11. J. Wu and L. Gao, "Dynamic energy management of fuel cell supercapacitor hybrid power systems for electric vehicles," *IEEE Transactions on Vehicular Technology*, vol. 65, no. 3, pp. 6892–6902, 2016.
12. J. D. Navamani, K. Vijayakumar, and R. Jegatheesan, "Non-isolated high gain DC-DC converter by quadratic boost converter and voltage multiplier cell," *Ain Shams Engineering Journal,* vol. 9, no. 4, pp. 1397–1406, 2018.